How do tectonics influence the initiation and evolution of submarine canyons? A case study from the Otway Basin, SE Australia

Nan Wu[1*], Harya D. Nugraha[2], Michael J. Steventon[3], Guangfa Zhong[1]

[1]State Key Laboratory of Marine Geology, Tongji University, Shanghai 200092, China

[2]Center for Sustainable Geoscience, Universitas Pertamina, Jakarta, 12220, Indonesia

[3]Shell Research, Shell Centre, London, SE1 7NA, UK.

*Email: nanwu@tongji.edu.cn

Abstract

The architecture of canyon-fills can provide a valuable record of the link between tectonics, sedimentation, and depositional processes in submarine settings. In this study, we investigate the role of plate tectonics in the initiation and evolution of submarine canyons. We demonstrate that plate tectonic-scale events (i.e. continental breakup and shortening) have a first-order influence on submarine canyon initiation and development. Initially, the Late Cretaceous (c.65 Ma) separation of Australia and Antarctica resulted in extensional fault systems, which then formed a steep stair-shaped paleo-seabed. Subsequently, the Late Miocene (c.5 Ma) collision of Australia and Eurasia has resulted in substantial uplift and exhumation in the SE Australian continental margin. These tectonic events have resulted in elevated seismicity that ultimately gave rise to the gravity-driven processes (i.e. turbidity currents and mass wasting processes) and formed the canyon base. The inherited stair-shaped topography then facilitated gravity-driven processes which established a mature sediment conduit extending from the shallow marine shelf to the abyssal plain. We indicate that the canyon stratigraphic architecture can be used as an archive to record tectonic movements. Moreover, the factors which preconditioned and triggered gravity-driven processes can also induce canyon initiation and facilitate canyon development.

Keywords: Submarine buried canyons; Mass wasting processes; Canyon-fill; Tectonic activity

1. Introduction

Submarine canyons are ubiquitous in deep-water settings and have long been considered as one of the major conduits for transporting sediment from the shelf edge, across the continental slope, and into the deeper abyssal plain (Shepard, 1981; Normark et al., 2003; Antobreh and Krastel, 2006). They are normally characterised by U-shaped cross-sectional geometries, that represents incision of hundreds of metres into the underlying stratigraphy, extend for several kilometres in width, and up to hundreds of kilometres long (i.e. Lewis and Barnes, 1999; Baztan et al., 2005; Su et al., 2020). When buried, the coarse-grained canyon-fill (i.e. sand-rich turbidites) may act as reservoirs for hydrocarbons and/or long-term carbon storage, in many submarine settings, (e.g. the South China Sea (Gong et al., 2011; Su et al., 2014), the Gulf of Mexico (Posamentier and Kolla, 2003), and SE offshore Australia (Moore et al., 2000; Tassone et al., 2014)).

The architecture and stratigraphic evolution of buried canyons contain a rich record of tectonics, sedimentation, and depositional process interactions in submarine settings. Previous studies have examined the evolution of canyon-fills from large-scale outcrop analogues, which provided valuable information on sedimentary facies and generally 2D depositional models of canyon-fills (i.e. Campion et al., 2003; Di Celma, 2011; Hodgson et al., 2011; Zecchin et al., 2011; McArthur and McCaffrey, 2019; Zecchin and Caffau, 2020; Janocko and Basilici, 2021). In addition, seismic reflection data-based studies have contributed significantly to our understanding of the three-dimensional architectural and long-term evolutionary trends of the canyon-fills (i.e. Rasmussen, 1994; Gong et al., 2011; He et al., 2013; Maier et al., 2018; Su et al., 2020). However, very few published studies have investigated how regional tectonics (i.e. plate tectonic-scale events) influence the initiation and evolution of submarine canyons. The controlling mechanisms of tectonic events behind the submarine canyons initiation and canyon-fills evolution remain poorly constrained.

This study focuses on the Otway Basin, located on the south-eastern Australian margin (Figure 1a). The modern seabed bathymetry is characterised by a low gradient (0.4^{o} to 1^{o}) continental shelf, and a steep (10^{o} to 30^{o}) continental slope that is transacted by multibranched canyons and regional distributed mass-transport complexes (MTCs) (Figure 1b; Leach and Wallace, 2001; Wu et al., 2022). In this study, we present two deeply buried, isolated cut and fill canyons (BC-1 and BC-2) that were formed in the Late Miocene, at a time when the Australian Plate collided with the Eurasian Plate. The high-resolution seismic reflection data from offshore SE Australia have provide an opportunity to constrain the relationship between plate tectonics and submarine canyon systems. We aim to: (i) investigate the canyon architectural evolution and depositional processes, and (ii) infer the influences of regional tectonics on canyon initiation and evolution. The detailed examination conducted in this study has important implications for understanding the principle controls of plate-scale tectonics in submarine canyons initiation and evolution, as well as provide an analogue for comparison to other submarine canyon systems.

2. Geological setting

2.1 Structural Framework

The Otway Basin is an NW-striking rift basin located on the south-eastern South Australia passive margin (Figure 1a, 1b). The basin was initiated by rifting during the Late Jurassic to early Palaeogene and formed due to the eventual continental separation between Antarctica and Australia during the break up of Gondwana at the end of the Cretaceous (Figure 2; Willcox and Stagg, 1990; Perincek and Cockshell, 1995; Norvick and Smith, 2001; Krassay et al., 2004). Since the Jurassic, the Otway Basin has had two significant phases of extensional tectonism, including a Late Jurassic-Early Cretaceous rifting phase and a Late Cretaceous rifting phase (Perincek and Cockshell, 1995; Krassay et al., 2004). The post-rift stage of the Otway Basin commenced in the Late Cretaceous, and most of the major faulting and tectonic activities associated with the final separation of Australia and Antarctica Plate ceased at that time (Krassay et al., 2004; Holford et al., 2014). The Late Jurassic- Early Cretaceous rifting phase has created an intense faulting event that affects the entire Cretaceous succession (Figure 3; Moore et al., 2000). The Cretaceous fault systems are generally NW-SE striking normal faults with an average dip of 60^{o} (Figure 3; Ziesch et al., 2017). These extensional faults normally terminate in the overlying thin Cenozoic succession and are characterised with high-angle extensional faults that dominant the shallower part of the basin, lower angle listric faults are common in the deeper part of the basin (Figure 3). The final breakup of the Australia and Antarctica Plates has resulted in a regionally distributed unconformity surface (Horizon H1 in this study) which separates the underlying Cretaceous and overlying Cenozoic successions (Figure 2, Figure 3; Krassay et al., 2004).

During the Late Miocene to Early Pliocene, the collision between the Indo-Australian plate and the Eurasian Plate generated long-wavelength (of the order 10^3 km) intraplate forces (Hillis et al., 2008; Tassone et al., 2012; Tassone et al., 2014). With the continuous collision, the NE boundary of the

Australian Plate exhibits complex structural styles, with the oceanic crust being subducted at Sumatra-Java Trench and the continental crust colliding along the Banda Arc and New Guinea (Figure 1a; Hillis et al., 2008). The collisional plate boundary segments have exerted an important control on the intraplate forces (Hillis et al., 2008). The Southern Australia margin has recorded the intraplate forces and experienced intensive uplift, exhumation, and deformation as indicated by both structural and sedimentological studies (Figure 3; Dickinson et al., 2002; Sandiford, 2003; Hillis et al., 2008). In Otway Basin, the distant intraplate forces reached their peak during Late Miocene to Early Pliocene, as evidenced by c. 5% crustal shortening yield strain rates (Cooper and Hill, 1997; Hillis et al., 2008; Holford et al., 2011), elevated levels of seismicity (Holford et al., 2011; Tassone et al., 2014), and substantial exhumation and uplift with magnitudes as high as c. 1 km within the Late Miocene-Early Pliocene successions (Holford et al., 2010). The onset of this late Miocene phase is marked by a regional unconformity (Horizon H2 in this study; Figure 2) that can be traced for more than 1500 km along the deep-water sedimentary basins in SE Australia (Dickinson et al., 2002; Tassone et al., 2014).

2.2 Sedimentology

The study interval lies in the Cenozoic stratigraphy in a passive continental margin setting. During the Cenozoic, the Otway Basin was in an open marine depositional environment, characterised by marine-related, calcareous-rich sediments (McGowran et al., 2004). The strata of the Cenozoic succession comprises of: the Wangerrip Group, the Nirranda Group, the Heytesbury Group, and the Whalers Bluff Formation (Figure 2; Perincek and Cockshell, 1995; Krassay et al., 2004; Totterdell et al., 2014). The Wangerrip Group (late Palaeocene to middle Eocene) represents the beginning of the passive margin sedimentation after the cessation of Late Cretaceous rifting (Figure 2). It unconformably overlies the regional Late Cretaceous unconformity (Horizon H1) and comprises of siliciclastic rich sediments (Figure 2). The Nirranda Group (middle Eocene to early Oligocene) is a succession of fine-grained siliciclastic in the lower section and marls in the upper section (Figure 2). The Heytesbury Group (late Oligocene to late Miocene) is deposited in fully marine conditions dominated by a combination of calcareous mudstone and mixed marine limestone (Figure 2; Ziesch et al., 2017). The Late Miocene to Pliocene tectonic inversion induced the deposition of fluvial sands, which continues up to the present day (Norvick and Smith, 2001). The Whalers Bluff Formation (WBF, Pliocene-Recent; Figure 2) mainly consists of siliciclastic-rich sediments and is mostly developed near the continental slope area (Tassone et al., 2011).

3. Dataset and Methodology

3.1 Dataset

A Geoscience Australia Database is used as the primary data source for this work, including high-resolution 2D and 3D seismic reflection data that was acquired by Santos in 2002 (Figure 1b). The 2D seismic data covers an area of approximately 5500 km^2, with the dominant frequency ranging from 20 to 30 Hz in the interval of interest. The 3D seismic-reflection dataset (OS02 3D) covers an area of c. 773 km^2, with a bin spacing of 25 m × 12.5 m (inline × crossline), and a dominant frequency of 35 Hz within the interval of interest. The 3D seismic data is zero-phase and presented in SEG normal polarity with an increase in acoustic impedance expressed as a positive amplitude (Figure 4). Given an average velocity of 2450 m/s within the interval of interest, we estimate the vertical resolution of the 2D seismic data ranges from approximately 20-30 m, and the 3D seismic data is approximately 17.5 m. The seismic reflection data encompass the modern continental shelf to continental slope area (Figure 1b). As shelf progradation occurs seaward since Miocene times, the Miocene shelf edge is located c. 50 km landward of the modern shelf edge (Figure 1b; Leach and Wallace, 2001). Therefore, the seismic datasets provide the opportunity to investigate the evolutional history of buried canyons and the tectonic features in a deep submarine setting.

3.2 Methodology

The age of the buried canyons was determined by correlations with offset wells (Figure 3) described in nearby studies (Leach and Wallace, 2001). We identified and interpreted three key horizons (H1, H2, and seabed), based on their high continuity (which extend throughout the study area) and strong amplitude. Schlumberger Petrel Software® is used to interpret seismic reflection data for this study. Horizon H1 (Figure 3, Figure 4) is a regionally mappable unconformity that has been correlated to the Late Cretaceous unconformity surface (Holford et al., 2014), and which records the eventual separation of the Australian and Antarctic Plates (Krassay et al., 2004; Holford et al., 2014). Horizon H2 (Figure 4, Figure 5) is another regionally mappable unconformity that has been tied to the Late Miocene unconformity surface, which formed due to the tectonic uplift and the associated canyon erosion (Holdgate et al., 2000; Dickinson et al., 2001; Leach and Wallace, 2001).

Five seismic facies are identified based on their external geometry, internal configuration, seismic amplitude, continuity, and seismic reflection termination patterns (Figure 6). The seismic facies interpretation is further guided by comparing their expression with previous seismic facies analysis schemes developed for buried submarine canyon-fills in the nearby area (Leach and Wallace, 2001) and in similar basin settings (Mayall et al., 2006; Gong et al., 2011; Mauffrey et al., 2017; Maier et al., 2018). A variance (coherency) attribute was calculated to illustrate and delineate the morphology and internal structures of the intra-canyon depositional elements. Variance attribute calculates the variability of a trace to its neighbour over a particular sample interval and produces interpretable lateral changes in acoustic impedance (Van Bemmel and Pepper, 2000), low variance response represents similar traces, and high variance response represents discontinuities (Brown, 2011). Therefore, coupled with seismic facies analyses, variance attributes can contribute to better imaging and mapping intra-canyon deposits.

4. Result

4.1 Seismic facies

Seismic facies-1: Turbidite complexes

Seismic facies-1 (SF-1) consists of parallel to sub-parallel, continuous, high amplitude seismic reflections (Figure 6). SF-1 typically displays onlapping or pinching out geometries toward the canyon sidewalls (Figure 6). SF-1 can be observed in most of the canyon cross-sectional profiles, it comprises approximately 5-10% of the buried canyon stratigraphy. SF-1 is c. 60-90 m thick and preferentially occurs at the base of the canyon fill. It is abundant in the lower section of the buried canyons and becomes less obvious in the middle and upper sections. Based on the seismic characteristics and previous seismic facies-based studies, SF-1 is interpreted as primarily coarse-grained turbidite complexes, representing multiple episodes of turbidity currents deposition (i.e. Cross et al., 2009; Gong et al., 2011; Wu et al., 2022).

Seismic facies-2: Background slope deposits

Seismic facies-2 (SF-2) is characterised by sheet-like, medium- to low-amplitude, laterally continuous reflections that cap SF-1 and SF-3 (Figure 6). SF-2 consists of a flat base and top surface with fair cross-sectional continuity, and no erosive features have been observed. In general, the SF-2 preferentially occurs at the middle part of the canyon-fill, and makes up c. 20% of the buried canyon stratigraphy. The thickness of SF-2 is constant, ranging from 150-190 m. Based on the seismic characteristics and previous seismic facies-based studies, SF-2 is interpreted as a mix of fine-grained turbidite complexes and mud-rich hemipelagic deposits (Symons et al., 2017; Maier et al., 2018), representing a low-energy depositional environment (Prather et al., 1998).

Seismic facies 3: Mass transport complexes (MTCs)

Seismic facies-3 (SF-3) consists of a discontinuous to chaotic reflection package with high- to medium-amplitude seismic reflections (Figure 6). The SF-3 is c. 170-300 m thick, has a rugose top surface and a relatively flat base surface (Figure 6). It dominates the middle to upper canyon-fill, representing nearly 60% of the buried canyon stratigraphy. The chaotic nature of the SF-3, combined with the rugose upper surface, indicates SF-3 has been remobilised and transported, mostly as MTCs (Prather et al., 1998; Posamentier, 2005; Steventon et al., 2019; Wu et al., 2019; Nugraha et al., 2019). Based on its seismic reflection character, we propose that SF-3 was initially deposited as and ultimately sourced from the remobilisation of SF-1 and SF-2.

Seismic facies 4: Turbidite channel

Seismic facies-4 (SF-4) is defined by medium-high amplitude, and has a bowl-shaped external form with an erosional base (Figure 6). Internal reflections of SF-4 are characterised by chaotic, medium amplitude reflection. Seismic reflections outside the SF-4 are of fare continuity and medium-high amplitude reflections (Figure 6). The thickness of SF-4 ranges from 130-170 m, it is observed primarily in the upper section of the canyon-fill, representing c. 5% of the buried canyon stratigraphy. The internal amplitudes of SF-4 are higher than that of the surrounding seismic facies, which indicates a higher acoustic impedance contrast when compared with surrounding facies. The erosional nature at the base of SF-4 suggests incisions, and the high amplitude of the fill might suggest that SF-4 is dominated by sandstone-rich deposits. We interpret SF-4 as turbidite channel deposits, as indicated by studies from Perov and Bhattacharya (2011) and Posamentier and Kolla (2003).

Seismic facies 5: Contourite channel

Seismic facies-5 (SF-5) is defined by sub-parallel to wavy, low-high amplitude seismic reflections, with truncated internal reflections (Figure 6). SF-5 can be easily recognised in the uppermost section of the buried canyons, near the continental shelf edge, having an elongated mounded shape and an adjacent concave moat (Figure 6). Based on its seismic reflection character, SF-5 is interpreted as contourites that are affected/reworked by contourite currents (Stow et al., 2002; Stow and Faugères, 2008; Rebesco et al., 2014).

4.2 The buried canyons

The buried canyons (BC-1 and BC-2) are deposited in the Oligocene to Miocene Heytesbury Group, and belong to Miocene Canyon systems which are defined by Leach and Wallace (2001). The BC-1 and BC-2 are S-oriented in the upper segment and SSW-oriented in the Lower segment (Figure 7a, 7b). The BC-1 is broad U-shaped canyons in seismic cross-section, ranging from c. 3 km to 5 km wide and cutting approximately c. 300 m to 500 m deep (Figure 8a-d). It is bounded by a lower undulatory erosional surface (Horizon H2) that truncates the underlying strata, showing a distinct seismic amplitude with negative polarity (Figure 4, Figure 8). The U-shaped erosional surfaces represent the oldest period of erosion and can be identified on most of the canyon cross-sectional profiles. The canyon sidewalls are steep, ranging from 20^{o} to more than 30^{o} (Figure 8). A series of sliding blocks are locally modified and truncated the steep canyon sidewalls, and located along the canyon margin (Figure 8c, 8d). The sliding blocks are bounded by strong amplitudes, with a negative polarity surface at the top, and positive polarity surface at the base (Figure 8d). The intra-sliding blocks are characterised by chaotic seismic facies that are similar to those defining canyon sidewall strata outside of the sliding blocks (Figure 8d). Moreover, the top and the base surfaces of the sliding blocks can be correlated into the canyon sidewall strata (Figure 8d).

The seismic facies assemblage of the sliding blocks is similar and can be correlated to the undeformed strata adjacent to the canyon walls, and is therefore interpreted to fail along the canyon sidewalls (Figure 8d). After the formation of the U-shaped erosional canyon base, the accommodation is filled by several different seismic facies. Based on the seismic facies infill pattern and their location toward the slope, the BC-1 is divided into two transverse segments (Upper segment and Lower segment; Figure 7b). The Upper segment starts from the upper (NW) gap of the 3D seismic data to the lower edge of the paleo-slope. The Lower segment covers most of the 3D seismic data area, expanding from the lower slope to the abyssal plain. In the following section, we take BC-1 (the biggest buried canyon in the study area) as an example to further investigate its facies association and infill patterns.

4.3 Canyon architecture

Upper segment

The upper segment of the BC-1 truncates into the paleo-lower continental slope (Figure 7a, 7b). The maximum width and relief of the buried canyon is c. 3 km and 300 m, respectively. In this segment, the lowermost and the uppermost section of the buried canyon is commonly filled with SF-1, suggesting that turbidite complexes are the most dominant depositional elements during the initial and final phase of the buried canyon-fill (Figure 8a, 8b). The upper section of the buried canyon filled is commonly SF-2, suggesting that hemipelagic deposits are deposited shortly after the turbidite complexes (Figure 8a, 8b). In the uppermost part of the canyon-fill, the SF-5 are present, indicating the contourite current activities have influenced the final stage of the canyon-fill (Figure 8a).

Lower segment

The Lower segment is SSW-oriented and constitutes the portion of the buried canyons where major accumulation took place. The width of the canyon in this segment is up to c. 7 km, with maximum sidewall reliefs of c. 500 m (Figure 8c, 8d). In the 3D seismic data area, most of the canyon-fill of the BC-1 is characterised by SF-3, which can constitute more than 70% of the canyon stratigraphy, with only thin (c. 30 m) deposition of SF-1 and SF-2 deposited in the middle or upper parts of the stratigraphy (Figure 8c, 8d). Further downslope, regional 2D seismic lines image several other buried canyons that deposited in the deeper submarine setting, with the percentage of the SF-3 infill increasing to nearly 90% of the total canyon stratigraphy (Figure 9a, 9b). The large percentage SF-3 infill show MTCs are the largest component of the Lower segment infill. A relatively thin fill (c. 90 m to 200 m) of turbidite complexes and background slope deposits appears in the upper section of the buried canyons.

The thick accumulation of MTCs indicate the Lower segment represents the part of the buried canyons where the intensity of erosion reached its peak (Figure 9a, 9b). The lower section of the canyon-fill was likely eroded by MTCs and preserved as erosional remnants scattered throughout the canyon-fill lower section (Figure 8c). The presence of the erosional remnants indicates the erosive MTCs has been initiated and transported from the Upper segment, and ultimately deposited in the Lower segment where extensive erosion is normal.

4.4 Intra-canyon MTCs

Several vertically stacked MTCs have been observed from the seismic sections cutting through the Lower segment of the BC-1. We map three seismically distinctive MTCs (MTC-1 to MTC-3; Figure

8c, 8d) to investigate the morphological and kinematic properties of these intra-canyon MTCs.

MTC-1 is bounded by horizons H2.1 and H2.2, it is laterally confined by the canyon base surface (Horizon H2) and mainly consisting of chaotic seismic facies with high amplitude seismic reflections (Figure 8c, 8d). MTC-1 is 90 to 130 m thick, being thickest near the canyon centre, and progressively thins towards and onlaps onto the canyon sidewalls (Figure 8c, 8d). In plain view, the distribution of MTC-1 is spatially confined within the BC-1, the lateral margins of MTC-1 follow an NNE-orientated direction, coinciding with the orientation of BC-1 sidewalls (Figure 10a). MTC-2 is 120 to 190 m thick and bounded by horizon H.2.2 and H2.3, and it contains chaotic seismic facies with medium amplitude reflections (Figure 8c, 8d). The lateral margins of MTC-2 follows an NNE-orientated direction, subparallel to the orientation of canyon sidewalls. Similar to MTC-1, MTC-2 is laterally confined by the Horizon H2 and spatially distributed within the area of the BC-1 (Figure 10b). MTC-3 is 130 to 210 m thick, and it is bounded by horizon H2.3 and H2.4, mainly consisting of chaotic seismic facies with medium amplitude reflections (Figure 7c, 7d). MTC-3 has NNE-orientated lateral margins, and the distribution of this MTC is nearly the same extent as the BC-1 (Figure 10c).

The orientation of NNE-striking lateral margins suggests these MTCs were transported towards the SSE. Although there is no direct evidence indicating the source area of MTCs, the overall distribution (confined within the lower section of canyon-fills) and the nature of the seismic facies, together suggest MTC-1, MTC-2, and MTC-3 may derive from the failures of turbidite complexes or background sediments that originally deposited in the Upper canyon segment. The strictly confined nature of the intra-canyon MTCs indicates that the distribution of these failures is controlled by the canyons' morphology (i.e. the width and the height). Compared with MTC-1, the areal extent of MTC-2, and MTC-3 is larger, which suggests mass failure processes become more dominant with the evolution of canyon-fill. We interpret that the reoccurrence of vertically stacked intra-canyon MTCs is associated with the intensive tectonic activities (i.e. faulting and tilting) in the continental shelf area during Late Miocene to Pliocene faults reactivation, which has been variously ascribed to the contemporaneous collision of Australia's northern margin with the island arc in New Guinea (Figure 1a; Hill et al., 1995).

5. Discussion

5.1 Sedimentological evolution of buried canyons

Based on the canyon-fill pattern, the evolutionary model of the buried canyons identified in the Otway Basin can be summarised into three stages: (i) mass wasting processes dominated the erosional-depositional stage, (ii) turbidites dominated the depositional stage, and (iii) a mixed mass wasting and -turbidite dominated erosional-depositional stage.

At the initial erosional stage, the morphology of the U-shaped canyon base has been attributed to the erosion by multiple mass failure events, as recorded by the thick deposition of MTCs in the distal section of the canyon-fill (Figure 9a, 9b). Another interpretation for the formation of the canyon base is the turbidity currents shaped the canyon and where then remobilised as MTCs. As turbidite complexes (or channel lags; Mayall et al., 2006) were observed at the lowermost section of the canyon-fill (Figure 9a). Due to the steep angle of the canyon sidewall (dips from c.40° to 60°), sidewall initiated sliding also occurs at the initial erosional stage. In the second depositional stage, processes such as turbidity currents and background sedimentations take place. The repeated cutting and filling by turbidity currents is one of the major features of canyon-fill, and the canyon-fill remains stable, similar to depositional patterns that have been recorded in other fills (i.e., Deptuck et al., 2007; Gong et al., 2011; Liang et al., 2020). In the final erosional-depositional stage, the canyon fill is dominated by the deposition of MTCs and turbidite channels. Contourite currents may play a role in the final stage of the canyon evolution. However, it is confined to the upper slope region, where the contourite currents are stronger than other current regimes (i.e. turbidity or mass-transport processes). For example, in the Upper segment of the canyon-fill (Figure 8a), the uppermost of the canyon-fill contains a large portion of contourite drifts and shows a distinct pattern similar to the examples from the South China sea and offshore Argentina where contourite activities are intense (i.e. He et al., 2013; Warratz et al., 2019).

5.2 Origin of the buried canyons

The causal mechanisms by which submarine canyons in the shallow submarine settings are initiated are generally a combination of near shelf-edge fluvial erosion during periods of relative sea-level fall/and or higher sediment flux (i.e. Posamentier et al., 1991) and retrogressive slope failure events occurring near the upper slope (i.e. Coleman et al., 1983; Goodwin and Prior, 1989;

Pratson and Coakley, 1996; He et al., 2014). The strong contourite current, tidal current activities, and hurricanes and typhoons, that occur near the coast may also play a role in the canyon initiation (i.e. Shepard et al., 1974; Sequeiros et al., 2019).

In the study area, the oldest buried Miocene canyons are tied to occur near the base of the Heytesbury Group (Leach and Wallace, 2001). Therefore, the initiation of the buried canyons likely started during the Late Miocene, when cool-water carbonates dominated (Leach and Wallace, 2001). The canyon bases are with high rugosity and show clear erosional features (Figure 8d) that are similar to those (i.e. grooves or scours) observed from the basal shear surface of MTCs (i.e.Bull et al., 2009; Butler et al., 2016). The Lower segment of the buried canyon-fill is characterised by a dominant deposition of MTCs, and the proportion of MTCs infill constantly increases toward to the farther distal part. Therefore, the origin of the buried canyons is tied to the occurrence of erosive gravity-driven processes (most likely mass wasting processes) during Late Miocene.

5.3 How do Late Miocene tectonics dictate the canyon initiation?

During Late Miocene, the SE Australia margin has experienced an extremely intense episode of uplift event, where the study area has experienced the most (Dickinson et al., 2001; Dickinson et al., 2002; Tassone et al., 2012). The driving mechanism for this uplifting episode is crustal shortening controlled intra-plate stresses, triggered by the northward movement of the Australia Plate towards the subduction zones along the northern boundary of the Indo-Australia plate (Figure 1a; i.e. Sandiford, 2007; Hillis et al., 2008). Such a momentous uplift event has generated a significant net exhumation around the deep-water Otway Basin during Late Miocene. For example, the gross exhumation in the submarine Otway Basin is more than 1000 m during Late Miocene to Pliocene (Green et al., 2004), near the study area, the gross exhumation could reach more than 1500 m (Duddy, 1997; Tassone et al., 2014). The significant exhumation has created an increase in onshore sediment supply and elevated levels of seismicity in the continental region (Dickinson et al., 2001). These changes have increased sediment instability in the upper slope and, consequently, gave rise to mass failure events (Sandiford, 2003; Sandiford et al., 2004). The above mentioned processes associated with the continental margin uplifting are marked by a regional erosion surface that can be traced for c. 1500 km along with SE Australia (Dickinson et al., 2002; Tassone et al., 2012). This is especially the case in the deep submarine where the regional erosion surface is corresponded to the extremely irregular canyon base surface (Horizon H2), and the canyon-fills are observed to display a thick package of chaotic seismic facies, indicating deposition of MTCs (Figure 9).

The Late Miocene erosion period corresponds to the time when the entire shelf was exposed and thus heavily incised by frequent deposition of MTCs, that were transported down to the deeper part of the basin. We infer that mass failures during episodes of intense tectonic, rather than other factors, caused of incision on the continental slope to initiate the development of buried canyons. The Late Miocene tectonics have helped establish a mature sediment conduit system that extended from shallower marine down to the abyssal plain.

5.4 How do Late Cretaceous tectonics influenced the canyon evolution?

The late Cretaceous fault systems are generally NW-SE striking (Figure 11a, 11b; Ziesch et al., 2017). The dip- and cross-seismic sections have revealed these faults cutting vertically beneath the thalwegs of the BC-1 and BC-2 (Figure 4b, 5b, 9b). The seismic dip line along the canyon axis shows the presence of the faults has created a stair-shaped structure within the Lower segment, which is truncated by the canyon (Figure 5b, 9b). The seismic dip line along the area outside the buried canyons show that after deposition of the pre-canyon succession (sedimentation between horizon H1-H2), the paleo-seafloor (at the time of H2) may have inherited the geometry created by the Cretaceous fault systems, showing a stair-shaped structure with a high-gradient (Figure 11c). This can be clearly seen from the onlapping patterns of sediments onto the local topographically high created by buried faults (Figure 11c).

The stair shaped geometry is interpreted as the hanging walls of the deeply sourced fault systems may have created a local structure high on the Late Cretaceous seafloor when horizon H1 is deposited. The footwalls of the deeply sourced fault systems have created a local structure low on the Late Cretaceous seafloor (Figure 12a). After the burial, the buried footwalls acted as a local high (buried hanging walls are locally low), causing an elevation difference between two adjacent footwalls and hanging walls (Figure 12a). When the canyon initiates, the stair-shape paleo geometry can cause an immediate increase in currents (e.g., turbidity currents or debris flow) energy and erosivity, thus facilitating the canyon development (Figure 12b). The subsequent canyon-fills was also influenced by the inherited topography created by the previous canyon infill and the stair-shape canyon base (Figure 12c). In modern analogues, the local gradient variation of the seabed has played a key role in canyon evolution (e.g., expansion in canyon width and depth), as demonstrated by modern canyon systems (Qin et al., 2017; Wu et al., 2022). Therefore, we suggest that the late Cretaceous fault-controlled zones may have pre-determined the location of the canyons by facilitating the erosional downcutting during the formation of the canyon base, this influence has not been instantaneous, instead the impact on the canyon evolution can be felt as late as tens of million years (or more).

5.5 Implication

Previous studies show that the tectonically active settings tend to develop small-scale, short-lived canyons (Eyles and Lagoe, 1998), while canyons in tectonically stable passive margin settings tend to develop relatively large scale canyons which are active for longer periods (Coleman et al., 1983). However, we reveal that in the tectonically active regions, uplift and tilting due to tectonic deformation induce an increased in sediment supply and seismicity, which can promote mass failure events thus contribute significantly to the formation of large-scale submarine canyons. Therefore, we indicate that the factors which preconditioned and triggered mass-transport complexes can also induce canyon initiation and facilitate canyon development. We suggest that the plate tectonic scale events (i.e. continental breakup and shortening) have a first-order influence on the submarine canyon initiation and evolution. The impact from the regional tectonics to the buried canyons can be instantaneous (i.e. directly trigger canyoning processes), or their influence can also be postponed (i.e. indirectly influence the seabed topography thus the canyon geometry).

6. Conclusion

1. The interpretation of the seismic data reveals that the sedimentological evolution of buried canyons can be divided into: (i) a mass wasting processes dominated the erosional-depositional stage, (ii) a turbidite dominated depositional stage, and (iii) a mixed mass wasting processes-turbidites dominated erosional-depositional stage. We indicate that in the deeper submarine settings (i.e. lower continental slope or abyssal plain), the interplay of turbidity currents and mass failure events control the canyon sedimentological and architectural patterns.

2. The intimate association of the buried canyon base with the Late Miocene uplift events suggest that canyon inception was triggered by Miocene uplifting and associated upper slope instability. We suggest that repeated mass failure is the most likely driving mechanism of the buried canyon

inception, in conjunction with increased sediment flux due to exhumation of the margin.

3. We interpret the extensional faults associated with the late Cretaceous plate separation between Australia and Antarctica as responsible for the inception and evolution of the buried canyons by increasing the steepness of the paleo-seabed, thus controlling the canyon geometry and location.

4. Plate-scale tectonic events have a close link with the submarine canyon initiation and evolution processes. The influence from regional tectonic movements to the initiation of canyons may have been almost instantaneous (i.e. directly triggering canyoning processes), or their influence can also be delayed (i.e. indirectly influence the canyon geometry).

Figure Caption

Figure 1. Location map of the study area. (a) Regional map of Australia. The black box marks the area shown in Figure 1b. Solid triangles indicate the direction of subduction, black arrows indicate slab pull forces, white arrows indicate resisting continent-continent collisional forces. Abbreviations: CB=collisional boundary, SZ=subduction zone; IA=island arc. Figure 1a is modified from Hillis et al. (2008). (b) Zoom-in map of the study area showing the location of the city of Portland and the Otway Basin. The white lines represent 2D seismic reflection data, the black dotted line represents the location of the modern shelf edge and the inferred location of the Miocene continental shelf edge (modified from Leach and Wallace, 2001), and the red box represents the extent of the 3D seismic reflection dataset. The GEBCO_2014 bathymetry map was sourced from https://www.ngdc.noaa.gov/maps/autogrid/.

Figure 2. Stratigraphic and tectonic event chart for the study area, showing the key horizons mapped in the seismic data and major tectonic events in the study interval. This figure is modified from Krassay et al. (2004) and Perincek and Cockshell (1995). Horizon H1 has been correlated to the late-Cretaceous unconformity surface from Holford et al. (2014). Horizon H2 has been correlated to the late-Miocene unconformity surface from Hillis et al. (2008).

Figure 3. Large scale regional seismic section across the inner SE Australian shelf to the deeper abyssal plain, highlighting unconformity surfaces (H1 and H2), and basinward thickening of the Upper Cretaceous mega-sequence. See the location of this regional seismic profile in Figure 1b.

Figure 3 is originally downloaded and modified from the Regional Geology of the Otway Basin report, Geoscience Australia online Repository.

Figure 4. (a) W-E seismic cross-section through the 3D seismic data area (see Figure 1b for location). (b) Interpreted seismic cross-section, showing the key horizons, major faults, and the location of the buried canyons.

Figure 5. (a) N-S seismic dip-section through the 3D seismic data area (see Figure 1b for location). (b) Interpreted seismic dip-section, showing the key horizons and the major faults.

Figure 6. General seismic facies characteristics observed in this study.

Figure 7. (a) Isopach map of Horizon H2 within OS02 3D area. (b) interpreted sketch of Figure 7a, showing the morphology of buried canyons (BC-1 and BC-2).

Figure 8. (a) Seismic section across the Upper Segment of the BC-1, showing the location of BC-1 and Horizons H1 and H2, (b) Seismic section across the Upper Segment of BC-1, (c) Seismic section across the Lower Segment of BC-1, (d) Seismic section across the Lower Segment of the BC-1. See the location of this figure in Figure 7b, and see the uninterpreted, clean seismic sections in the supplementary material.

Figure 9. (a) 2D seismic section in the deep submarine settings imaging the buried canyons. (b) 2D seismic section shows the dip-section of the buried canyons. See location of this figure from Figure 1b, the uninterpreted seismic sections are available in the supplementary material.

Figure 10. (a) Variance attribute calculated on horizon H2.1, showing a map view of MTC-1. Note that the white dotted lines indicate the boundary of the buried canyon, and the yellow dotted lines indicate the boundary of MTCs. (b) Variance attribute calculated on horizon H2.2, showing a map view of MTC-2. (c) Variance attribute calculated on horizon H2.3, showing a map view of MTC-3. See the location of this figure in Figure 7b.

Figure 11. (a) Variance attribute map calculated on the horizon a (see the location of this horizon in Figure 11c), showing the extensional faults formed during the Late Cretaceous. (b). Interpreted view of Figure 11a, showing the location of the extensional faults (white dotted lines) and the location of the buried canyons (blue dotted lines). (c) Seismic cross-section through the area outside of the buried canyons (see Figure 11b for location). See an uninterpreted version of Figure 11c in the supplementary material.

Figure 12. Schematic figure showing the evolution model of the buried canyons. (a) Schematic

figure showing the regionally distributed Late Cretaceous extensional faults. (b) Schematic figure showing the initiation of the MTCs that formed the canyon bases during the Late Miocene. (c) Schematic figure showing the canyon-fill pattern after the formation of the canyon base.

Data Access

The data used in this study can be requested from the Geoscience Australia Repository https://www.ga.gov.au/data-pubs. In this study we used OS02 3D survey and OS02 2D survey. The GEBCO_2014 bathymetry map is downloaded from https://www.ngdc.noaa.gov/maps/autogrid/.

Reference

Antobreh, A.A.&Krastel, S., 2006. Morphology, seismic characteristics and development of Cap Timiris Canyon, offshore Mauritania: a newly discovered canyon preserved-off a major arid climatic region. Marine and Petroleum Geology, 23(1): 37-59.

Baztan, J., Berné, S., Olivet, J.-L., Rabineau, M., Aslanian, D., Gaudin, M., Réhault, J.-P.&Canals, M., 2005. Axial incision: The key to understand submarine canyon evolution (in the western Gulf of Lion). Marine and Petroleum Geology, 22(6-7): 805-826.

Brown, A.R., 2011. Interpretation of three-dimensional seismic data. Society of Exploration Geophysicists and American Association of Petroleum Geologists.

Bull, S., Cartwright, J.&Huuse, M., 2009. A review of kinematic indicators from mass-transport complexes using 3D seismic data. Marine and Petroleum Geology, 26(7): 1132-1151.

Butler, R.W., Eggenhuisen, J.T., Haughton, P.&McCaffrey, W.D., 2016. Interpreting syndepositional sediment remobilization and deformation beneath submarine gravity flows; a kinematic boundary layer approach. Journal of the Geological Society, 173(1): 46-58.

Campion, K.M., Sprague, A., Mohrig, D., Lovell, R., Drzewiecki, P., Sullivan, M., Ardill, J., Jensen, G.&Sickafoose, D., 2003. Outcrop expression of confined channel complexes.

Coleman, J.M., Prior, D.B.&Lindsay, J.F., 1983. Deltaic influences on shelfedge instability processes.

Cooper, G.&Hill, K., 1997. Cross-section balancing and thermochronological analysis of the Mesozoic development of the eastern Otway Basin. The APPEA Journal, 37(1): 390-414.

Cross, N.E., Cunningham, A., Cook, R.J., Taha, A., Esmaie, E.&El Swidan, N., 2009. Three-dimensional seismic geomorphology of a deep-water slope-channel system: The Sequoia field, offshore west Nile Delta, Egypt. AAPG bulletin, 93(8): 1063-1086.

Deptuck, M.E., Sylvester, Z., Pirmez, C.&O'Byrne, C., 2007. Migration–aggradation history and 3-D seismic geomorphology of submarine channels in the Pleistocene Benin-major Canyon, western Niger Delta slope. Marine and Petroleum Geology, 24(6-9): 406-433.

Di Celma, C., 2011. Sedimentology, architecture, and depositional evolution of a coarse-grained submarine canyon fill from the Gelasian (early Pleistocene) of the Peri-Adriatic basin, Offida, central Italy. Sedimentary Geology, 238(3-4): 233-253.

Dickinson, J., Wallace, M., Holdgate, G., Daniels, J., Gallagher, S.&Thomas, L., 2001. Neogene tectonics in SE Australia: implications for petroleum systems. The APPEA Journal, 41(1): 37-52.

Dickinson, J.A., Wallace, M.W., Holdgate, G.R., Gallagher, S.J.&Thomas, L., 2002. Origin and timing of the Miocene-Pliocene unconformity in southeast Australia. Journal of Sedimentary Research, 72(2): 288-303.

Duddy, I., 1997. Focussing exploration in the Otway Basin: understanding timing of source rock maturation. The APPEA Journal, 37(1): 178-191.

Eyles, C.H.&Lagoe, M.B., 1998. Slump-generated megachannels in the Pliocene–Pleistocene glaciomarine Yakataga Formation, Gulf of Alaska. Geological Society of America Bulletin, 110(3): 395-408.

Gong, C., Wang, Y., Zhu, W., Li, W., Xu, Q.&Zhang, J., 2011. The Central Submarine Canyon in the Qiongdongnan Basin, northwestern South China Sea: architecture, sequence stratigraphy, and depositional processes. Marine and petroleum Geology, 28(9): 1690-1702.

Goodwin, R.H.&Prior, D.B., 1989. Geometry and depositional sequences of the Mississippi Canyon, Gulf of Mexico. Journal of Sedimentary Research, 59(2): 318-329.

Green, P., Crowhurst, P.&Duddy, I., 2004. Integration of AFTA and (U-Th)/He thermochronology to enhance the resolution and precision of thermal history reconstruction in the Anglesea-1 well, Otway Basin, SE Australia.

He, Y., Xie, X., Kneller, B.C., Wang, Z.&Li, X., 2013. Architecture and controlling factors of canyon fills on the shelf margin in the Qiongdongnan Basin, northern South China Sea. Marine and Petroleum Geology, 41: 264-276.

He, Y., Zhong, G., Wang, L.&Kuang, Z., 2014. Characteristics and occurrence of submarine canyon-associated landslides in the middle of the northern continental slope, South China Sea. Marine and Petroleum Geology, 57: 546-560.

Hill, K.C., Hill, K.A., Cooper, G.T., O'Sullivan, A.J., O'Sullivan, P.B.&Richardson, M.J., 1995. Inversion around the Bass basin, SE Australia. Geological Society, London, Special Publications, 88(1): 525-547.

Hillis, R.R., Sandiford, M., Reynolds, S.D.&Quigley, M.C., 2008. Present-day stresses, seismicity and Neogene-to-Recent tectonics of Australia's 'passive'margins: intraplate deformation controlled by plate boundary forces. Geological Society, London, Special Publications, 306(1): 71-90.

Hodgson, D., Di Celma, C., Brunt, R.&Flint, S., 2011. Submarine slope degradation and aggradation and the stratigraphic evolution of channel–levee systems. Journal of the Geological Society, 168(3): 625-628.

Holdgate, G., Wallace, M., Gallagher, J.D.S., Keene, J.&Smith, A., 2000. Controls on Seaspray Group sonic velocities in the Gippsland Basin—a multi-disciplinary approach to the canyon seismic velocity problem. The APPEA Journal, 40(1): 293-313.

Holford, S., Hillis, R., Duddy, I., Green, P., Tuitt, A.&Stoker, M., 2010. Impacts of Neogene-Recent compressional deformation and uplift on hydrocarbon prospectivity of the passive southern Australian margin. The APPEA Journal, 50(1): 267-286.

Holford, S.P., Hillis, R.R., Hand, M.&Sandiford, M., 2011. Thermal weakening localizes intraplate deformation along the southern Australian continental margin. Earth and Planetary Science Letters, 305(1-2): 207-214.

Holford, S.P., Tuitt, A.K., Hillis, R.R., Green, P.F., Stoker, M.S., Duddy, I.R., Sandiford, M.&Tassone, D.R., 2014. Cenozoic deformation in the Otway Basin, southern Australian margin: Implications for the origin and nature of post-breakup compression at rifted margins. Basin Research, 26(1): 10-37.

Janocko, J.&Basilici, G., 2021. Architecture of coarse-grained gravity flow deposits in a structurally confined submarine canyon (late Eocene Tokaren Conglomerate, Slovakia). Sedimentary Geology, 417: 105880.

Krassay, A., Cathro, D.&Ryan, D., 2004. A regional tectonostratigraphic framework for the Otway Basin.

Leach, A.&Wallace, M., 2001. Cenozoic submarine canyon systems in cool water carbonates from the Otway Basin, Victoria, Australia.

Lewis, K.B.&Barnes, P.M., 1999. Kaikoura Canyon, New Zealand: active conduit from near-shore sediment zones to trench-axis channel. Marine Geology, 162(1): 39-69.

Liang, C., Xie, X., He, Y., Chen, H., Yu, X., Zhang, W., Mi, H., Lu, B., Tian, D.&Zhang, H., 2020. Multiple sediment sources and topographic changes controlled the depositional architecture of a palaeoslope-parallel canyon in the Qiongdongnan Basin, South China Sea. Marine and Petroleum Geology, 113: 104161.

Maier, K.L., Johnson, S.Y.&Hart, P., 2018. Controls on submarine canyon head evolution: Monterey Canyon, offshore central California. Marine Geology, 404: 24-40.

Mauffrey, M.-A., Urgeles, R., Berné, S.&Canning, J., 2017. Development of submarine canyons after the Mid-Pleistocene Transition on the Ebro margin, NW Mediterranean: The role of fluvial connections. Quaternary Science Reviews, 158: 77-93.

Mayall, M., Jones, E.&Casey, M., 2006. Turbidite channel reservoirs—Key elements in facies prediction and effective development. Marine and Petroleum Geology, 23(8): 821-841.

McArthur, A.D.&McCaffrey, W.D., 2019. Sedimentary architecture of detached deep-marine canyons: Examples from the East Coast Basin of New Zealand. Sedimentology, 66(3): 1067-1101.

McGowran, B., Holdgate, G., Li, Q.&Gallagher, S., 2004. Cenozoic stratigraphic succession in southeastern Australia. Australian Journal of Earth Sciences, 51(4): 459-496.

Moore, A., Stagg, H.&Norvick, M., 2000. Deep-water Otway Basin: a new assessment of the tectonics and hydrocarbon prospectivity. The APPEA Journal, 40(1): 66-85.

Normark, W.R., Carlson, P.R., Chan, M.&Archer, A., 2003. Giant submarine canyons: Is size any clue to their importance in the rock record? Special Papers-Geological Society of America: 175-190.

Norvick, M.&Smith, M., 2001. Mapping the plate tectonic reconstruction of southern and southeastern Australia and implications for petroleum systems. The APPEA Journal, 41(1): 15-35.

Nugraha, H. D., Jackson, C. A. L., Johnson, H. D., Hodgson, D. M., & Reeve, M. T. (2019). Tectonic and oceanographic process interactions archived in Late Cretaceous to Present deep-marine stratigraphy on the Exmouth Plateau, offshore NW Australia. *Basin Research*, *31*(3), 405-430.

Perincek, D.&Cockshell, C., 1995. The Otway basin: early Cretaceous rifting to Neogene inversion. The APPEA Journal, 35(1): 451-466.

Perov, G.&Bhattacharya, J.P., 2011. Pleistocene shelf-margin delta: Intradeltaic deformation and sediment bypass, northern Gulf of Mexico. AAPG bulletin, 95(9): 1617-1641.

Posamentier, H., Erskine, R.&Mitchum, R., 1991. Models for submarine-fan deposition within a sequence-stratigraphic framework, Seismic facies and sedimentary processes of submarine fans and turbidite systems. Springer, pp. 127-136.

Posamentier, H.W., 2005. Stratigraphy and geomorphology of deep-water mass transport complexes based on 3D seismic data, SEG Technical Program Expanded Abstracts 2005. Society of Exploration Geophysicists, pp. 2300-2303.

Posamentier, H.W.&Kolla, V., 2003. Seismic geomorphology and stratigraphy of depositional elements in deep-water settings. Journal of sedimentary research, 73(3): 367-388.

Prather, B.E., Booth, J.R., Steffens, G.S.&Craig, P.A., 1998. Classification, lithologic calibration, and stratigraphic succession of seismic facies of intraslope basins, deep-water Gulf of Mexico. AAPG bulletin, 82(5): 701-728.

Pratson, L.F.&Coakley, B.J., 1996. A model for the headward erosion of submarine canyons induced by downslope-eroding sediment flows. Geological Society of America Bulletin, 108(2): 225-234.

Qin, Y., Alves, T.M., Constantine, J.&Gamboa, D., 2017. The role of mass wasting in the progressive development of submarine channels (Espirito Santo Basin, SE Brazil). Journal of Sedimentary Research, 87(5): 500-516.

Rasmussen, E.S., 1994. The relationship between submarine canyon fill and sea-level change: an example from Middle Miocene offshore Gabon, West Africa. Sedimentary Geology, 90(1-2): 61-75.

Rebesco, M., Hernández-Molina, F.J., Van Rooij, D.&Wåhlin, A., 2014. Contourites and associated sediments controlled by deep-water circulation processes: State-of-the-art and future considerations. Marine Geology, 352: 111-154.

Sandiford, M., 2003. Neotectonics of southeastern Australia: linking the Quaternary faulting record with seismicity and in situ stress. Special Papers-geological Society of America: 107-120.

Sandiford, M., 2007. The tilting continent: a new constraint on the dynamic topographic field from Australia. Earth and Planetary Science Letters, 261(1-2): 152-163.

Sandiford, M., Wallace, M.&Coblentz, D., 2004. Origin of the in situ stress field in south-eastern Australia. Basin Research, 16(3): 325-338.

Sequeiros, O.E., Pittaluga, M.B., Frascati, A., Pirmez, C., Masson, D.G., Weaver, P., Crosby, A.R., Lazzaro, G., Botter, G.&Rimmer, J.G., 2019. How typhoons trigger turbidity currents in submarine canyons. Scientific reports, 9(1): 1-15.

Shepard, F.P., 1981. Submarine canyons: multiple causes and long-time persistence. AAPG bulletin, 65(6): 1062-1077.

Shepard, F.P., Marshall, N.F.&McLoughlin, P.A., 1974. " Internal Waves" Advancing along Submarine Canyons. Science, 183(4121): 195-198.

Steventon, M.J., Jackson, C.A.L., Hodgson, D.M.&Johnson, H.D., 2019. Strain analysis of a seismically imaged mass-transport complex, offshore Uruguay. Basin Research, 31(3): 600-620.

Stow, D.&Faugères, J.-C., 2008. Contourite facies and the facies model. Developments in sedimentology, 60: 223-256.

Stow, D.A., Faugères, J.-C., Howe, J.A., Pudsey, C.J.&Viana, A.R., 2002. Bottom currents, contourites and deep-sea sediment drifts: current state-of-the-art. Geological Society, London, Memoirs, 22(1): 7-20.

Su, M., Lin, Z., Wang, C., Kuang, Z., Liang, J., Chen, H., Liu, S., Zhang, B., Luo, K.&Huang, S., 2020. Geomorphologic and infilling characteristics of the slope-confined submarine canyons in the Pearl River Mouth Basin, northern South China Sea. Marine Geology, 424: 106166.

Su, M., Xie, X., Xie, Y., Wang, Z., Zhang, C., Jiang, T.&He, Y., 2014. The segmentations and the significances of the Central Canyon System in the Qiongdongnan Basin, northern South China Sea. Journal of Asian Earth Sciences, 79: 552-563.

Symons, W.O., Sumner, E.J., Paull, C.K., Cartigny, M.J., Xu, J., Maier, K.L., Lorenson, T.D.&Talling, P.J., 2017. A new model for turbidity current behavior based on integration of flow monitoring and precision coring in a submarine canyon. Geology, 45(4): 367-370.

Tassone, D., Holford, S., Tingay, M., Tuitt, A., Stoker, M.&Hillis, R., 2011. Overpressures in the central Otway Basin: the result of rapid Pliocene–Recent sedimentation? The APPEA Journal, 51(1): 439-458.

Tassone, D.R., Holford, S.P., Duddy, I.R., Green, P.F.&Hillis, R.R., 2014. Quantifying Cretaceous–Cenozoic exhumation in the Otway Basin, southeastern Australia, using sonic transit time data: Implications for conventional and unconventional hydrocarbon prospectivity. AAPG Bulletin, 98(1): 67-117.

Tassone, D.R., Holford, S.P., Hillis, R.R.&Tuitt, A.K., 2012. Quantifying Neogene plate-boundary controlled uplift and deformation of the southern Australian margin. Geological Society, London, Special Publications, 367(1): 91-110.

Totterdell, J., Bradshaw, M., Owen, K., Hashimoto, T.&Hall, L., 2014. Petroleum geology inventory of Australia's offshore frontier basins. Geoscience Australia.

Van Bemmel, P.P.&Pepper, R.E., 2000. Seismic signal processing method and apparatus for generating a cube of variance values. Google Patents.

Warratz, G., Schwenk, T., Voigt, I., Bozzano, G., Henrich, R., Violante, R.&Lantzsch, H., 2019. Interaction of a deep-sea current with a blind submarine canyon (Mar del Plata Canyon, Argentina). Marine Geology, 417: 106002.

Willcox, J.&Stagg, H., 1990. Australia's southern margin: a product of oblique extension. Tectonophysics, 173(1-4): 269-281.

Wu, N., Jackson, C.A.-L., Johnson, H., Hodgson, D.M.&Nugraha, H.D., 2019. Mass-transport complexes (MTCs) document minibasin subsidence patterns and diapir evolution in the northern Gulf of Mexico.

Wu, N., Nugraha, H.D., Zhong, G.&Steventon, M.J., 2022. The role of mass-transport complexes in the initiation and evolution of submarine canyons. Sedimentology.

Zecchin, M.&Caffau, M., 2020. Emergence of a submarine canyon, Crotone Basin, southern Italy. Marine and Petroleum Geology, 114: 104204.

Zecchin, M., Caffau, M.&Roda, C., 2011. Relationships between high-magnitude relative sea-level changes and filling of a coarse-grained submarine canyon (Pleistocene, Ionian Calabria, Southern Italy). Sedimentology, 58(4): 1030-1064.

Ziesch, J., Aruffo, C.M., Tanner, D.C., Beilecke, T., Dance, T., Henk, A., Weber, B., Tenthorey, E., Lippmann, A.&Krawczyk, C.M., 2017. Geological structure and kinematics of normal faults in the Otway Basin, Australia, based on quantitative analysis of 3-D seismic reflection data. Basin Research, 29(2): 129-148.

Figure 1

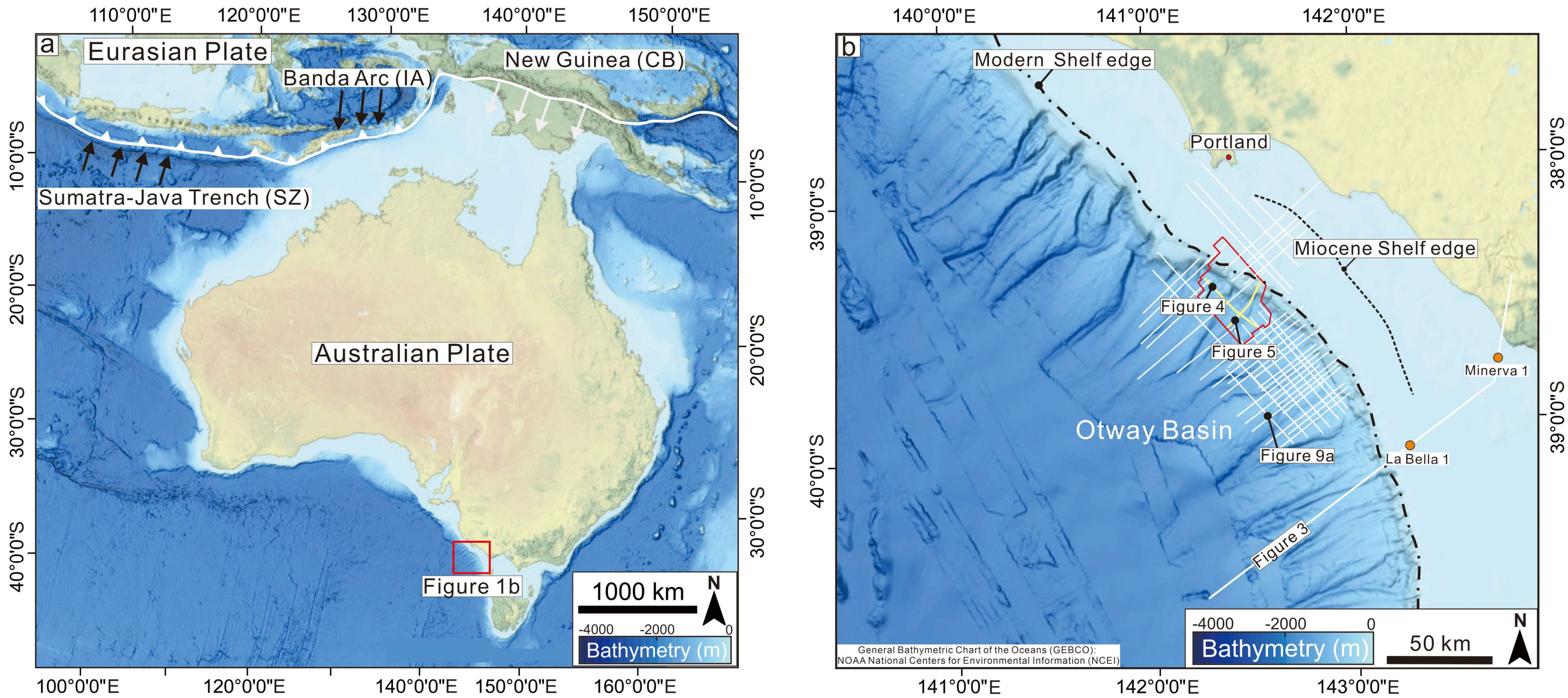

a
Eurasian Plate
Banda Arc (IA)
New Guinea (CB)
Sumatra-Java Trench (SZ)
Australian Plate
Figure 1b
1000 km
N
-4000 -2000 0
Bathymetry (m)
110°0'0"E
120°0'0"E
130°0'0"E
140°0'0"E
150°0'0"E
100°0'0"E
160°0'0"E
10°0'0"S
20°0'0"S
30°0'0"S
40°0'0"S
b
Modern Shelf edge
Portland
Miocene Shelf edge
Figure 4
Figure 5
Otway Basin
Figure 9a
Minerva 1
La Bella 1
Figure 3
-4000 -2000 0
Bathymetry (m)
50 km
N
General Bathymetric Chart of the Oceans (GEBCO):
NOAA National Centers for Environmental Information (NCEI)
140°0'0"E
141°0'0"E
142°0'0"E
143°0'0"E
38°0'0"S
39°0'0"S
40°0'0"S

Figure 2

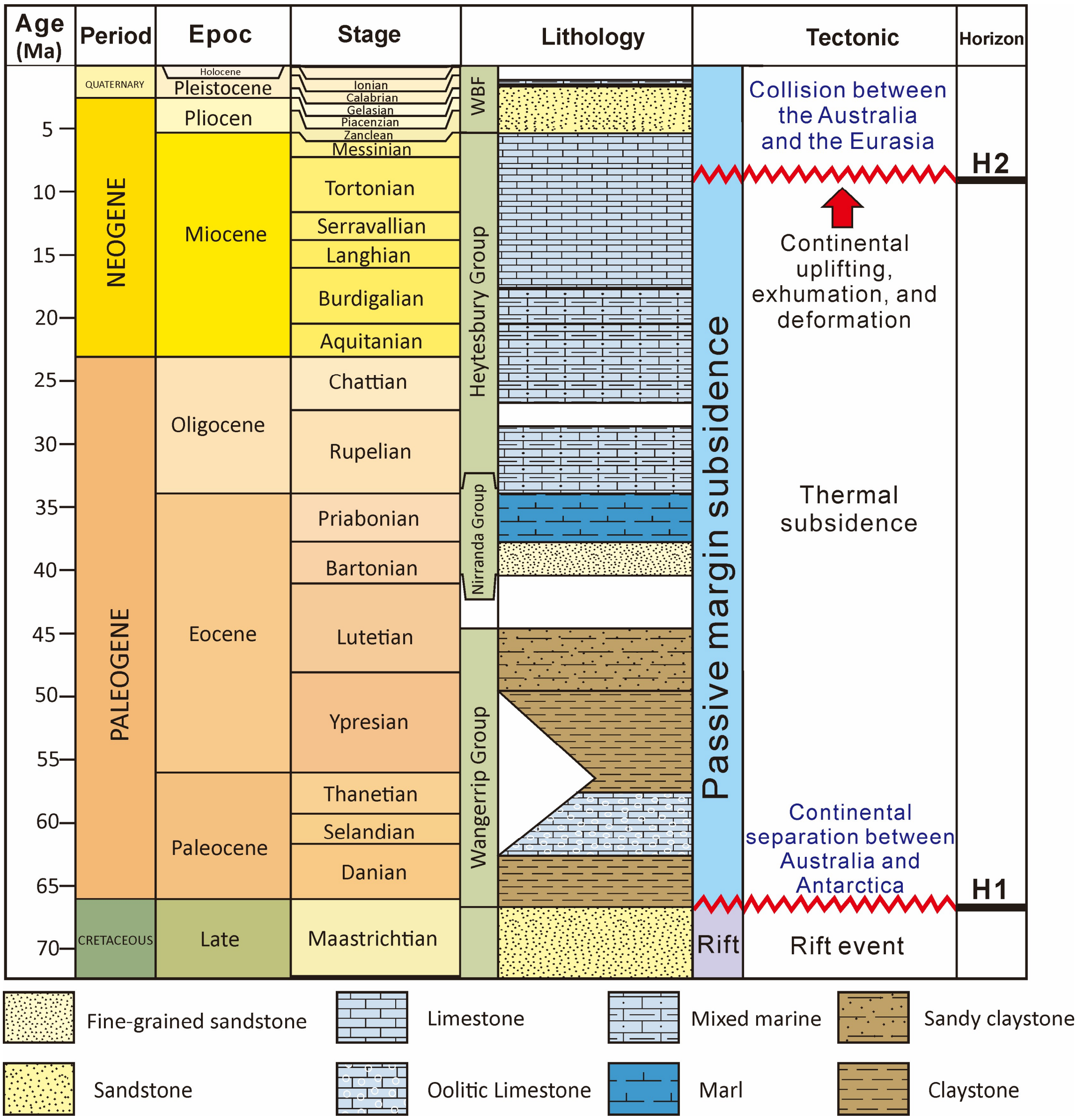

Age (Ma)
Period
Epoc
Stage
Lithology
Tectonic
Horizon
5
10
15
20
25
30
35
40
45
50
55
60
65
70
QUATERNARY
NEOGENE
PALEOGENE
CRETACEOUS
Holocene
Pleistocene
Pliocen
Miocene
Oligocene
Eocene
Paleocene
Late
Ionian
Calabrian
Gelasian
Piacenzian
Zanclean
Messinian
Tortonian
Serravallian
Langhian
Burdigalian
Aquitanian
Chattian
Rupelian
Priabonian
Bartonian
Lutetian
Ypresian
Thanetian
Selandian
Danian
Maastrichtian
WBF
Heytesbury Group
Nirranda Group
Wangerrip Group
Passive margin subsidence
Rift
Collision between the Australia and the Eurasia
Continental uplifting, exhumation, and deformation
Thermal subsidence
Continental separation between Australia and Antarctica
Rift event
H2
H1
Fine-grained sandstone
Limestone
Mixed marine
Sandy claystone
Sandstone
Oolitic Limestone
Marl
Claystone

Figure 3

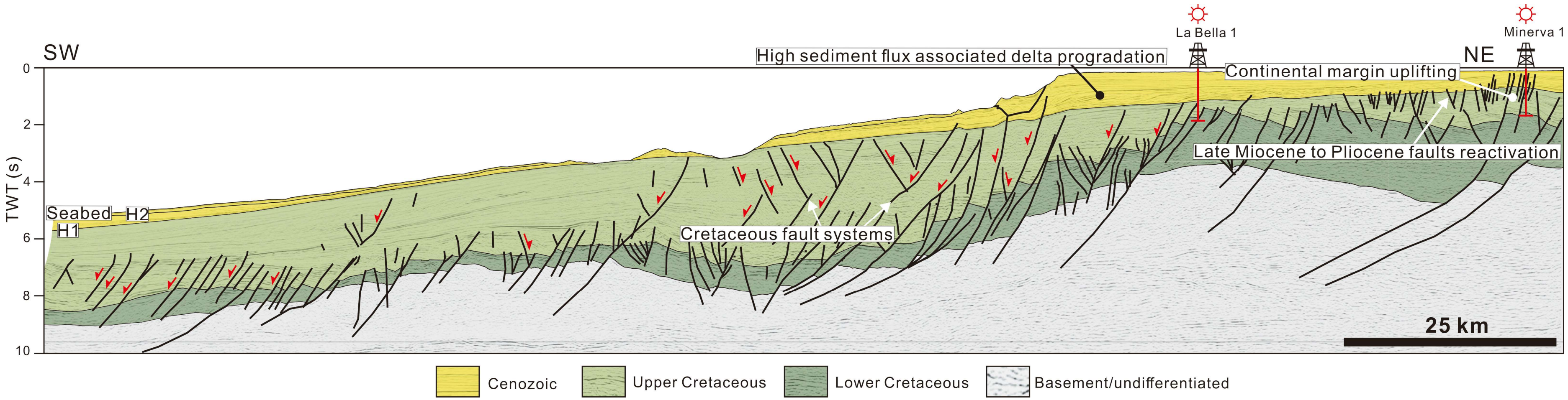

La Bella 1
Minerva 1
SW
NE
High sediment flux associated delta progradation
Continental margin uplifting
Late Miocene to Pliocene faults reactivation
Cretaceous fault systems
Seabed
H2
H1
TWT (s)
0
2
4
6
8
10
25 km
Cenozoic
Upper Cretaceous
Lower Cretaceous
Basement/undifferentiated

Figure 4

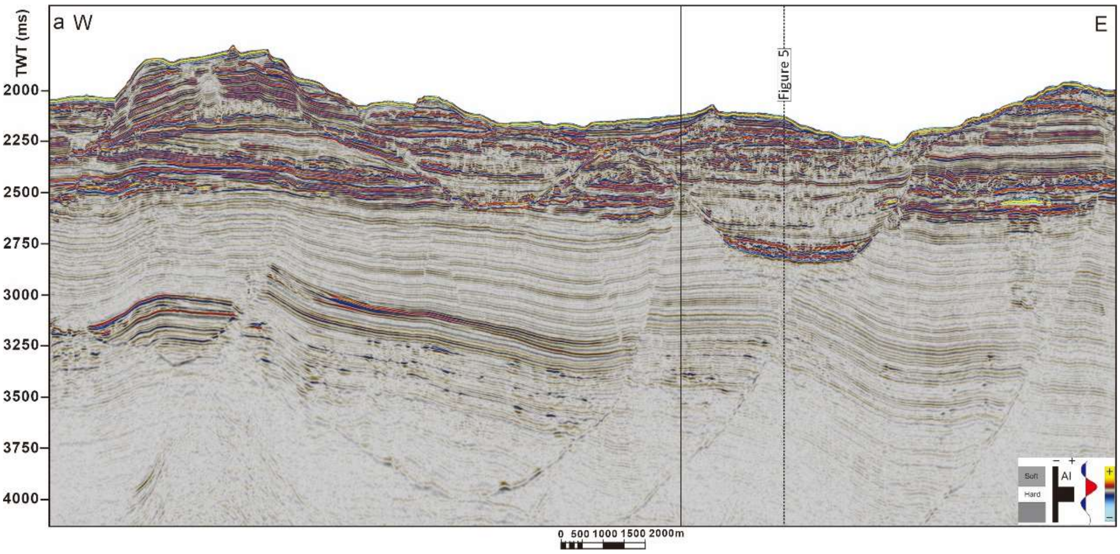

a W
E
TWT (ms)
2000
2250
2500
2750
3000
3250
3500
3750
4000
Figure 5
Soft
Hard
AI
0 500 1000 1500 2000m

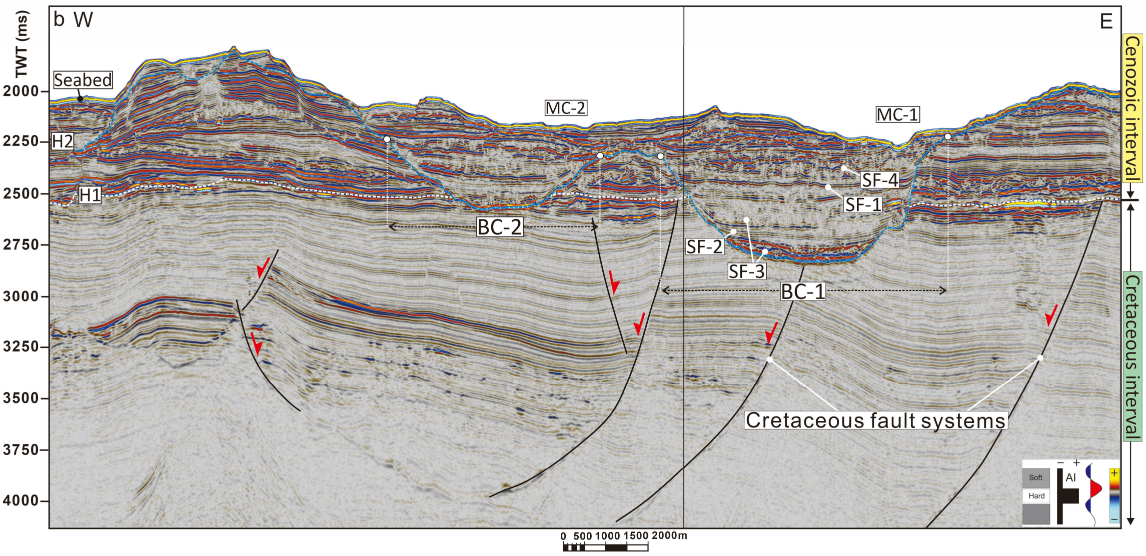

b W
E
TWT (ms)
Seabed
H2
H1
MC-2
MC-1
SF-4
SF-1
SF-2
SF-3
BC-2
BC-1
Cretaceous fault systems
Cenozoic interval
Cretaceous interval
2000
2250
2500
2750
3000
3250
3500
3750
4000
Soft
Hard
AI
0 500 1000 1500 2000m

Figure 5

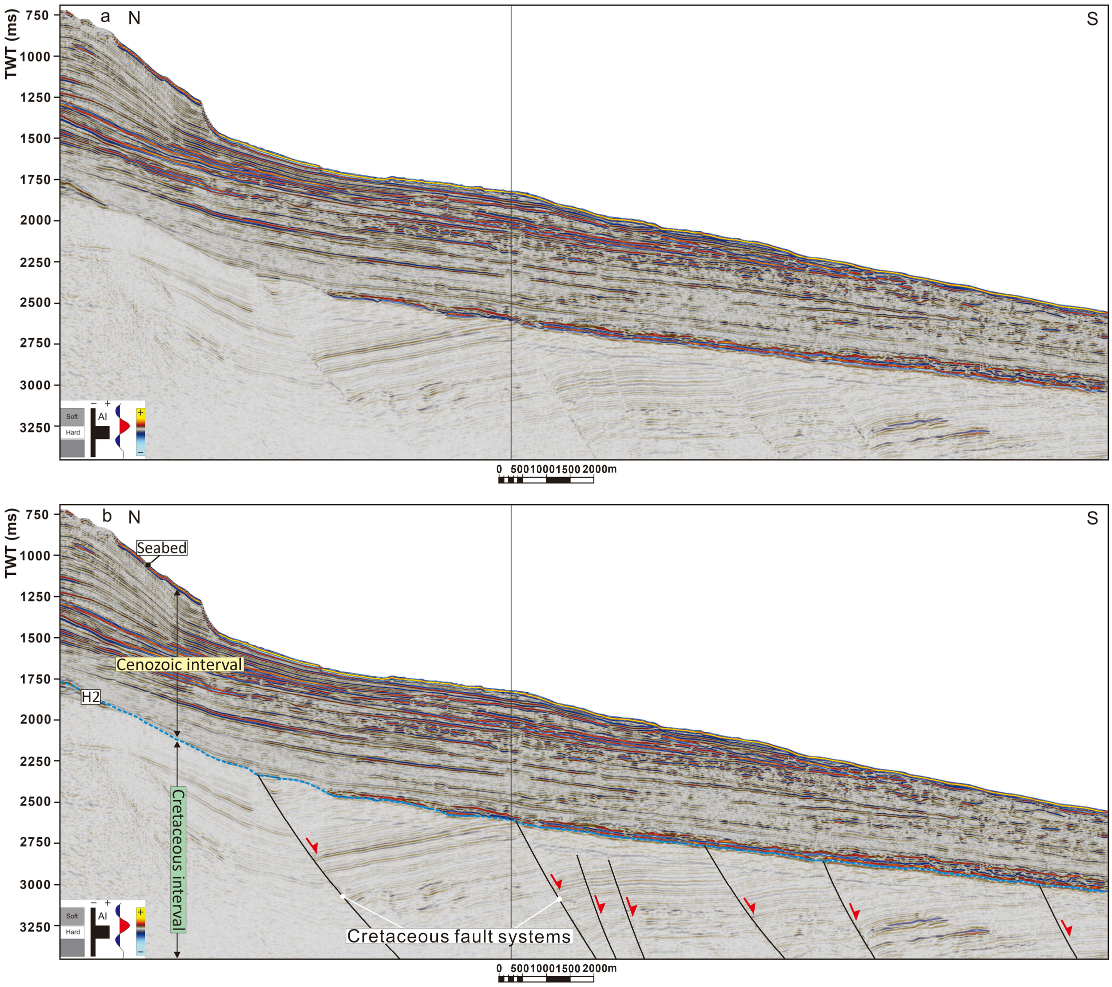

TWT (ms)
750
1000
1250
1500
1750
2000
2250
2500
2750
3000
3250
a
N
S
Soft
Hard
AI
0 500 1000 1500 2000m
b
Seabed
Cenozoic interval
H2
Cretaceous interval
Cretaceous fault systems

Figure 6

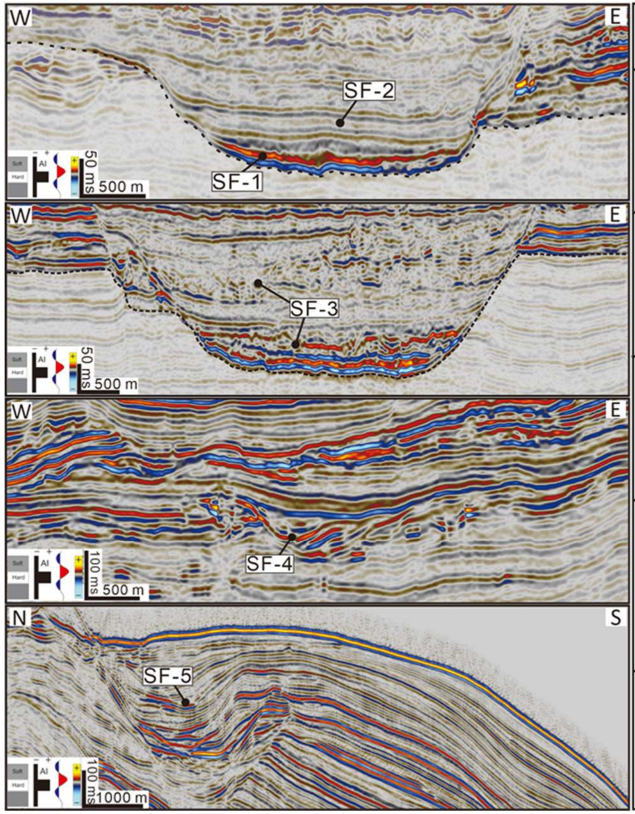

Facies	Description	Interpretation
SF-1	Internally coherent, high- to medium-amplitude, continuous seismic facies.	Turbidite complexes
SF-2	Internally coherent, medium- to low-amplitude, continuous seismic facies.	Hemipelagic sediment
SF-3	Internally deformed, medium- to high- amplitude reflections, trough-shaped seismic facies.	Mass-transport complexes (MTCs)
SF-4	Internally chaotic, medium- to high- amplitude reflections, bowl-shaped external form with an erosional base.	Turbidite channel
SF-5	Internally sub-parallel to wavy, low-high amplitude seismic reflections with truncated base surface.	Contourite channel

Figure 7

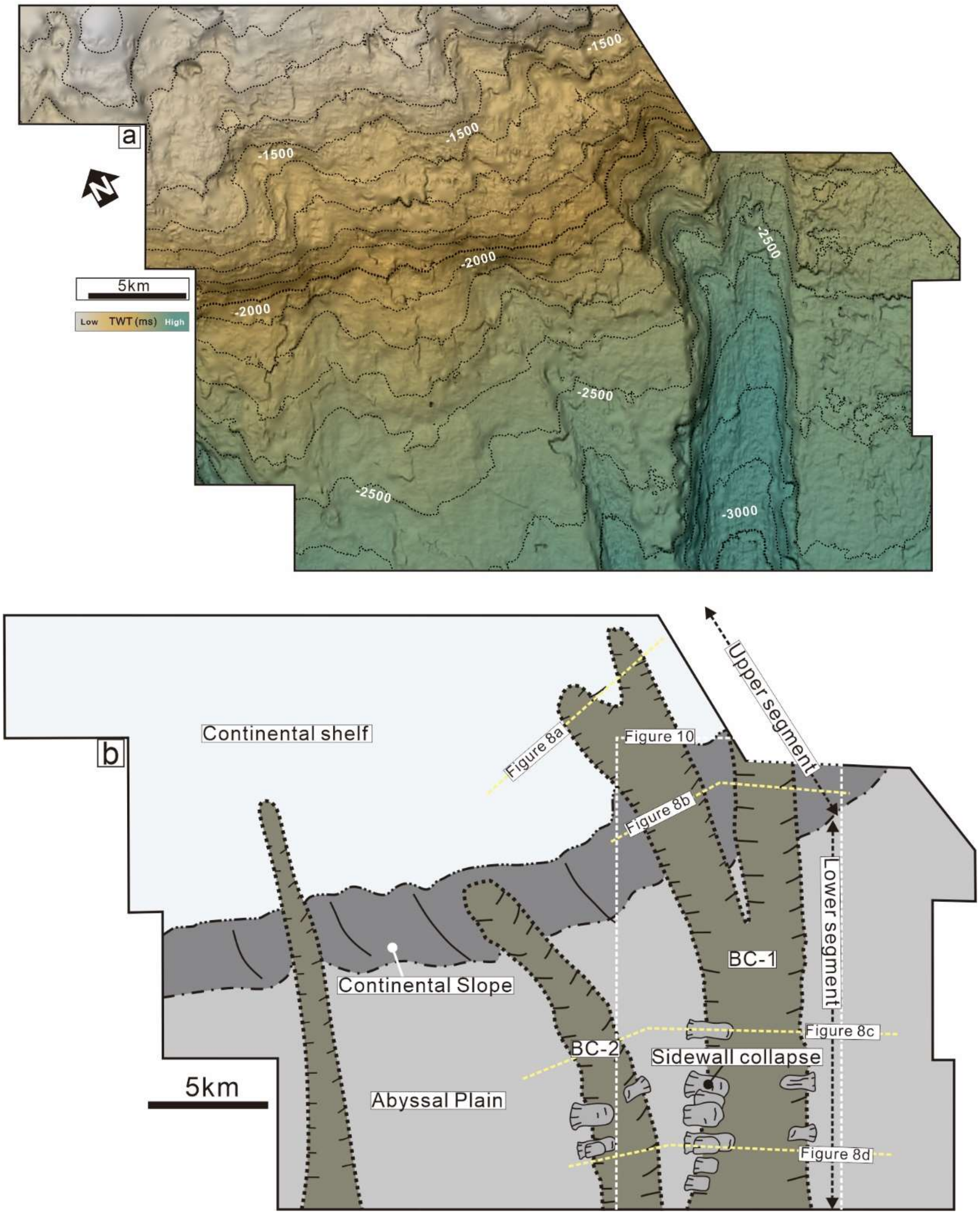
a
-1500
-1500
-1500
-2000
-2000
-2500
-2500
-2500
-3000
5km
Low TWT (ms) High
b
Continental shelf
Figure 8a
Figure 10
Upper segment
Figure 8b
Lower segment
Continental Slope
BC-1
BC-2
Figure 8c
Sidewall collapse
5km
Abyssal Plain
Figure 8d

Figure 8

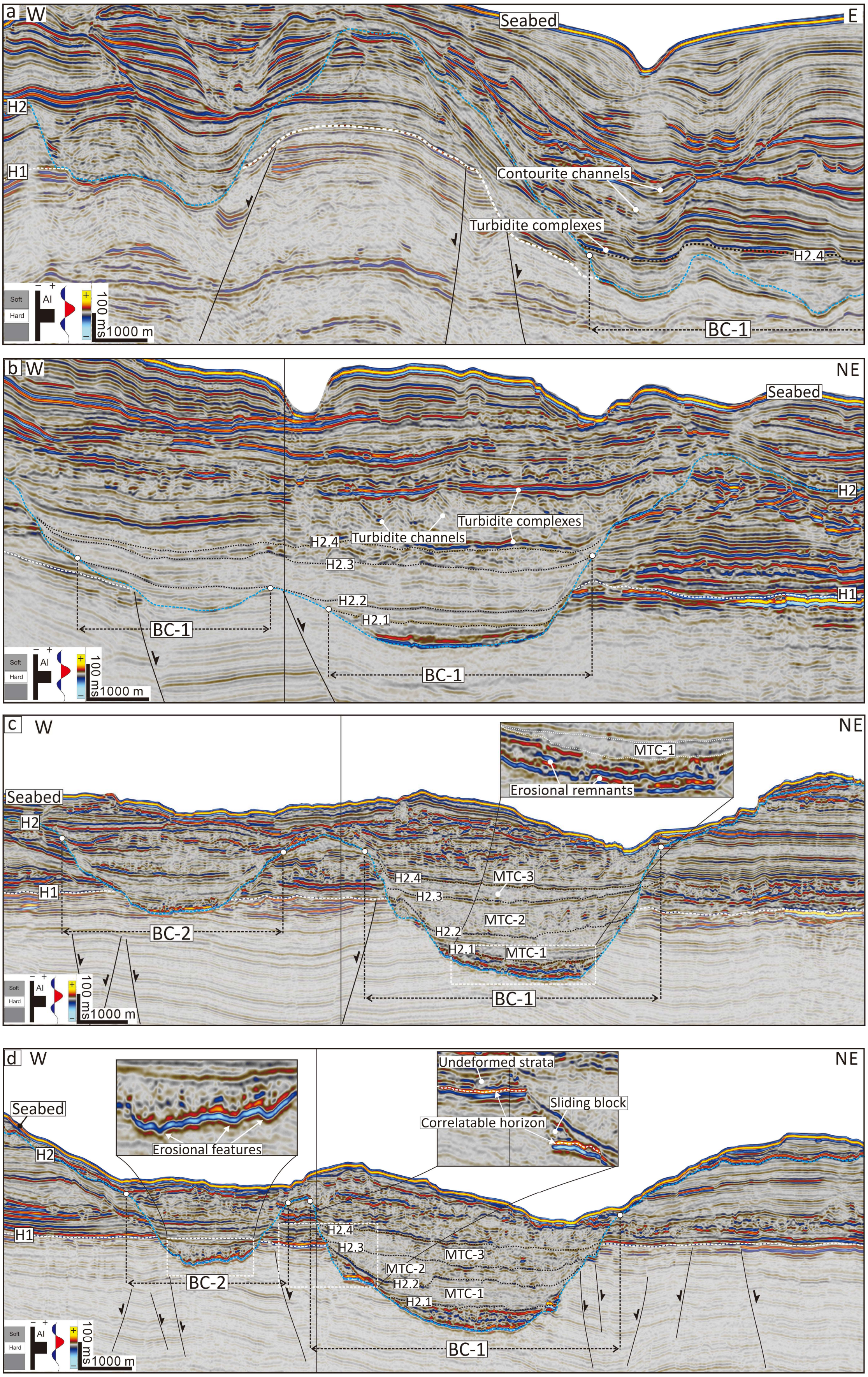

a
W
E
Seabed
H2
H1
Contourite channels
Turbidite complexes
H2.4
BC-1
Soft
Hard
AI
100 ms
1000 m
b
W
NE
Seabed
H2
H1
Turbidite complexes
Turbidite channels
H2.4
H2.3
H2.2
H2.1
BC-1
BC-1
100 ms
1000 m
c
W
NE
Seabed
H2
H1
MTC-1
Erosional remnants
MTC-3
MTC-2
MTC-1
H2.4
H2.3
H2.2
H2.1
BC-2
BC-1
100 ms
1000 m
d
W
NE
Seabed
H2
H1
Erosional features
Undeformed strata
Sliding block
Correlatable horizon
H2.4
H2.3
MTC-3
MTC-2
H2.2
H2.1
MTC-1
BC-2
BC-1
100 ms
1000 m

Figure 9

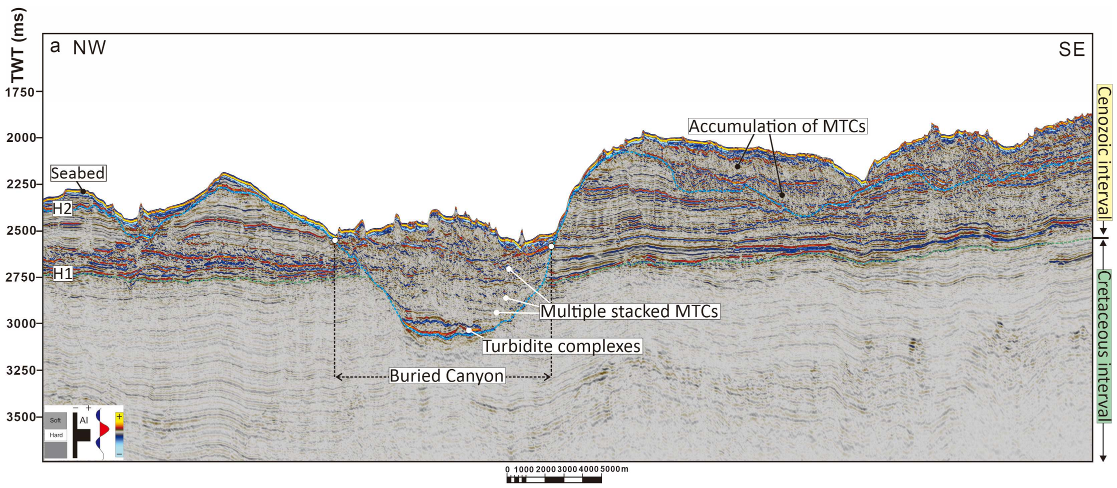

TWT (ms)
a NW
SE
Seabed
H2
H1
Accumulation of MTCs
Multiple stacked MTCs
Turbidite complexes
Buried Canyon
Cenozoic interval
Cretaceous interval
Soft
Hard
AI
0 1000 2000 3000 4000 5000m

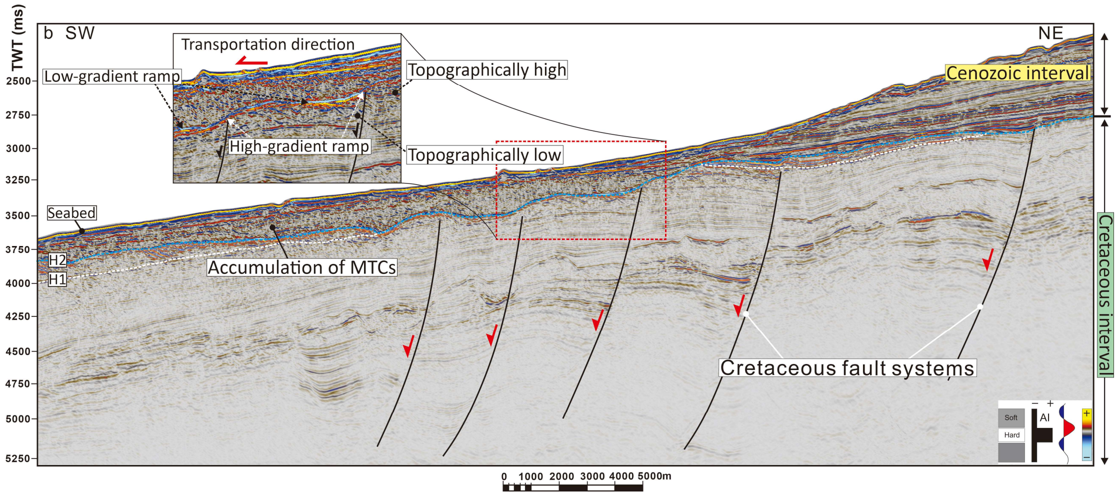

TWT (ms)
b SW
NE
Transportation direction
Low-gradient ramp
Topographically high
High-gradient ramp
Topographically low
Seabed
H2
H1
Accumulation of MTCs
Cretaceous fault systems
Cenozoic interval
Cretaceous interval
Soft
Hard
AI
0 1000 2000 3000 4000 5000m

Figure 10

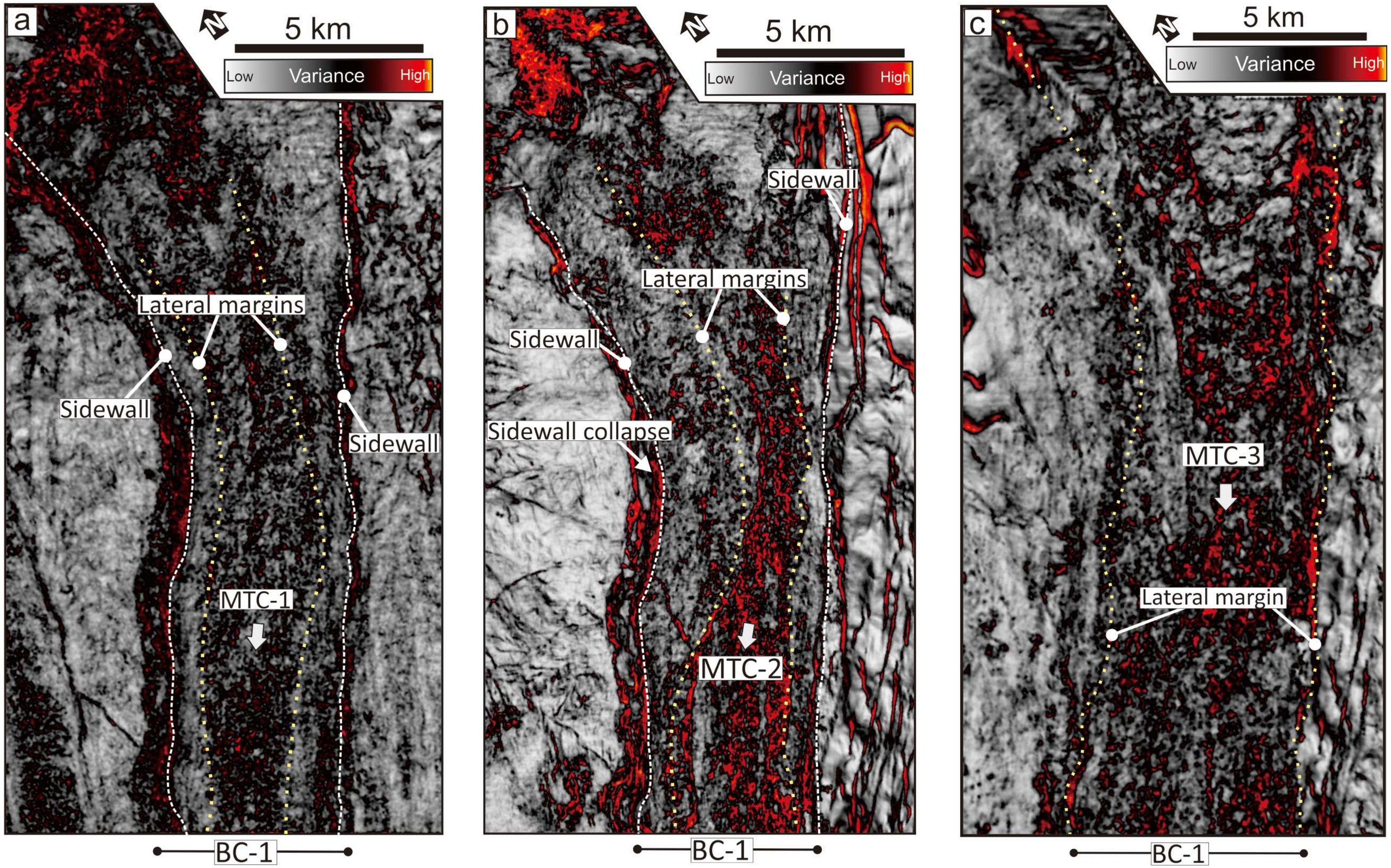

a
5 km
Low
Variance
High
Lateral margins
Sidewall
Sidewall
MTC-1
BC-1
b
5 km
Low
Variance
High
Sidewall
Lateral margins
Sidewall
Sidewall collapse
MTC-2
BC-1
c
5 km
Low
Variance
High
MTC-3
Lateral margin
BC-1

Figure 11

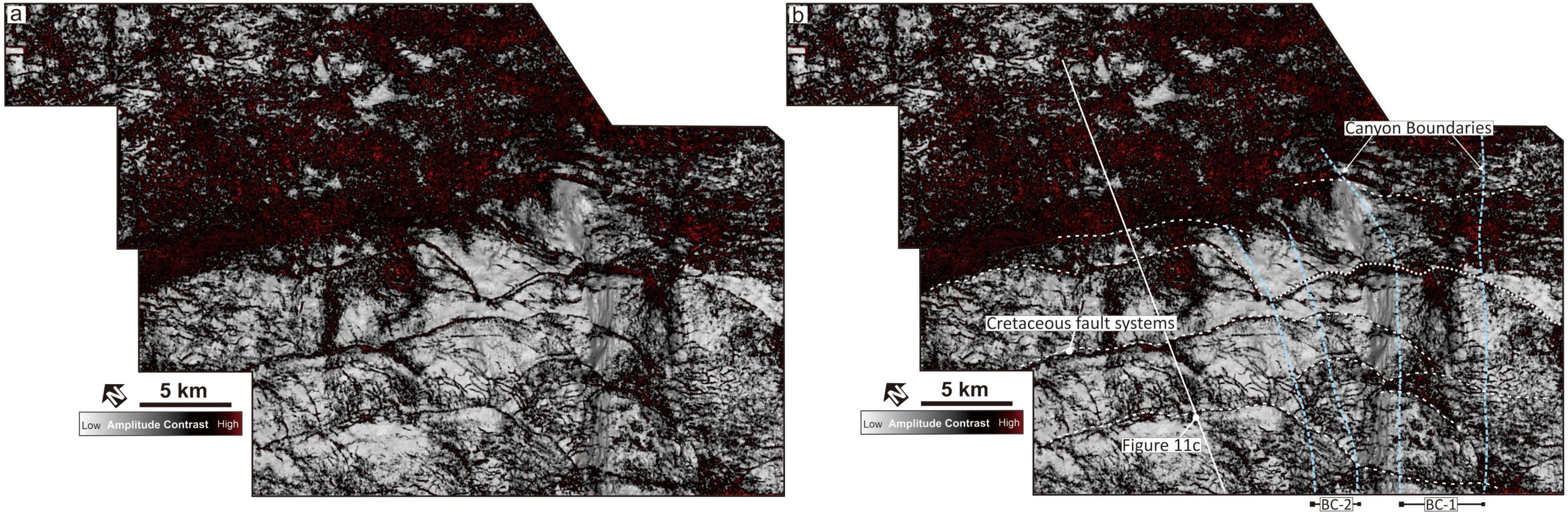
a
5 km
Low Amplitude Contrast High
b
Canyon Boundaries
Cretaceous fault systems
5 km
Low Amplitude Contrast High
Figure 11c
BC-2
BC-1

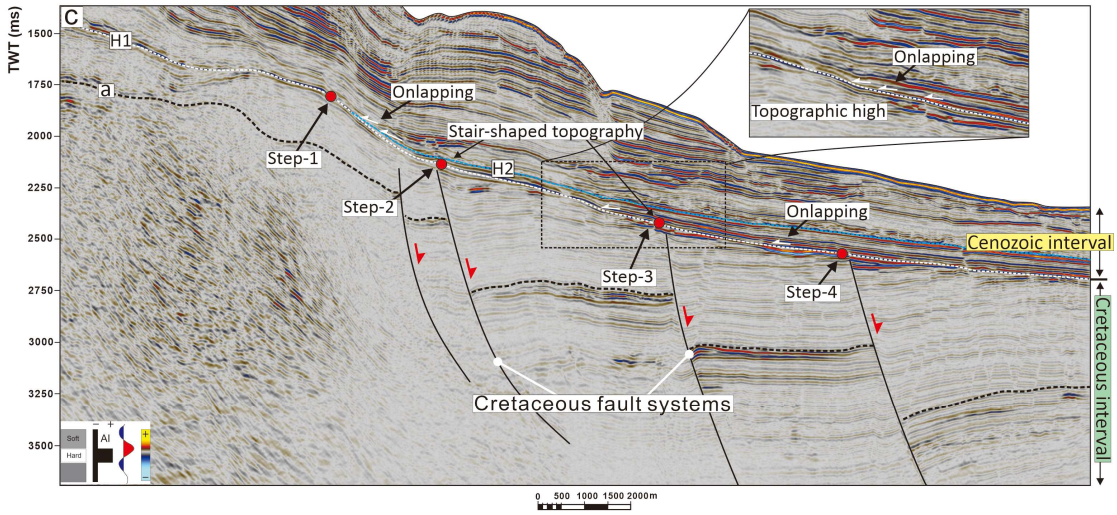

C
TWT (ms)
1500
1750
2000
2250
2500
2750
3000
3250
3500
H1
a
H2
Step-1
Step-2
Step-3
Step-4
Onlapping
Stair-shaped topography
Onlapping
Topographic high
Cenozoic interval
Cretaceous interval
Cretaceous fault systems
Soft
Hard
AI
0 500 1000 1500 2000m

Figure 12

T1: Late Cretaceous (c. 65 Ma): Continental separation between Australia and Antarctica